Nanoscale Shape and Size Control of Cubic, Cuboctahedral, and Octahedral Cu−Cu_2O Core−Shell Nanoparticles on Si(100) by One-Step, Templateless, Capping-Agent-Free Electrodeposition

Abdullah Radi,[†] Debabrata Pradhan, Youngku Sohn,[‡] and K. T. Leung*

WATLab and Department of Chemistry, University of Waterloo, Waterloo, Ontario N2L 3G1, Canada. [†]Present address: Department of Chemistry, University of British Columbia, Vancouver, B.C., Canada. [‡]Present address: Department of Chemistry, Yeungnam University, Gyeongsan, Gyeongbuk 712-749, South Korea.

ABSTRACT Cu−Cu_2O core−shell nanoparticles (NPs) of different shapes over an extended nanosize regime of 5−400 nm have been deposited on a H-terminated Si(100) substrate by using a simple, one-step, templateless, and capping-agent-free electrochemical method. By precisely controlling the electrolyte concentration [$CuSO_4 \cdot 5H_2O$] below their respective critical values, we can obtain cubic, cuboctahedral, and octahedral NPs of different average size and number density by varying the deposition time under a few seconds (<6 s). Combined glancing-incidence X-ray diffraction and depth-profiling X-ray photoelectron spectroscopy studies show that these NPs have a crystalline core−shell structure, with a face-centered cubic metallic Cu core and a simple cubic Cu_2O shell with a CuO outerlayer. The shape control of Cu−Cu_2O core−shell NPs can be understood in terms of a diffusion-limited progressive growth model under different kinetic conditions as dictated by different [$CuSO_4 \cdot 5H_2O$] concentration regimes.

KEYWORDS: Cu−Cu_2O core−shell nanoparticles · cubic · cuboctahedral · octahedral · shape and size control · electrodeposition · X-ray photoelectron spectroscopy

Between the two extremes of a single atom and the bulk, metallic nanoparticles (NPs) have many unique size-dependent properties, including quantum size effects, large surface area to volume ratios, and novel chemistry. As one of the best conductors of both heat and electricity, copper is used as a low-cost, versatile metal in many applications, including catalysis (*e.g.*, for methanol synthesis from CO_2 and H_2)[1] and microelectronics (*e.g.*, printed circuit boards and wiring).[2] In addition, the oxides of copper (*i.e.*, Cu_2O and CuO), which normally form on the outer shell of Cu NPs, also have numerous useful properties for catalysis,[1,3] fuel cells,[4] solar cells,[5] gas sensing,[6−8] and selective biofiltering for neutralizing and deactivating viruses.[9,10] To synthesize Cu and/or Cu_2O NPs with well-defined morphology and chemical composition, both physical methods (including chemical vapor deposition and laser ablation)[11,12] and chemical methods (including sol−gel, hydrothermal, and electrochemical deposition)[13−16] have been used. Of these, the solution-based route is quite attractive because it requires a lower synthesis temperature and has potential for large-scale production of NPs. In the solution-based route, two typical approaches are used to prepare NPs of different shapes and sizes.[17] In one approach, normally a template (soft or hard) is employed to physically confine the shape and size of NPs.[18−20] In the other approach, a capping agent is often used to control the growth direction and dimension of NPs.[16,21,22] As it is not always easy to completely remove the template materials and other additives used in the synthesis, preparation of purely single-phase NPs of well-defined shapes is limited. Similarly, the capping agents used to form a particular shape of Cu and/or Cu_2O NPs may play an undesirable role in the needed application. It is therefore highly beneficial to develop an alternative method to produce Cu and/or Cu_2O NPs of different shapes without the use of templates or capping agents. Here, we demonstrate, for the first time, a simple, one-step, templateless, and capping-agent-free method of synthesizing Cu−Cu_2O core−shell NPs with well-defined shapes and size distributions.

In the solution-based route, NPs can be either synthesized in powder form or deposited on a substrate. There are several reports on the synthesis of powder Cu and/or Cu_2O NPs, particularly with spherical or rod

*Address correspondence to tong@uwaterloo.ca.

Received for review January 5, 2010 and accepted February 9, 2010.

Published online February 18, 2010.
10.1021/nn100023h

shape, by using a solution-based method.[15,23−25] Indeed, the formation of Cu NPs and clusters on different substrates using a variety of different methods has been reported extensively in the literature, and these substrates include organic and polymer surfaces,[26−34] metallic surfaces,[35,36] and Si(100)[37−39] and Si(111)[40−42] surfaces. However, the number of reports about Cu or Cu−Cu_2O core−shell NPs on Si substrates is limited and largely to the nucleation and growth of Cu NP clusters without any attempt to control the shape.[37−42] Another novelty of the present work therefore lies in the shape control of NPs (with different exposed facets) specifically on the industrially relevant Si substrate. As Cu_2O NPs with different exposed facets can behave differently and exhibit different catalytic properties,[43] it is of fundamental and commercial interest to grow different shapes of Cu_2O NPs on a Si substrate. Among the several solution-based techniques used to grow NPs, electrochemical deposition represents a low-cost, flexible, scalable method extensively used for growing NPs with definite morphology and chemical composition on a variety of substrates, including low-heat-tolerant materials (*e.g.*, plastics and polymers).[44] For example, Oskam *et al.* studied the nucleation and growth mechanism of Cu on n-type Si from sulfate solution, and they found that Cu undergoes progressive nucleation growth on the Si surface, forming islands according to the Wolmer−Weber model.[45] Grujicic and Pesic studied the nucleation of Cu on a glassy carbon substrate also in a sulfate solution, and they found that the pH, concentration of the copper electrolyte, deposition potential, temperature, and supporting electrolyte all influence the nucleation and growth of the NPs differently.[46] Ko *et al.* produced triangular pyramidal Cu NPs on gold by using an organic capping reagent that limits the growth of the (111) plane,[36] while Tang *et al.* produced octahedral particles on the gold surface.[35] In our previous studies, we studied the deposition of cubic Cu NPs on polypyrrole films electrochemically deposited on either a gold electrode[32,33] or a gold film sputter-coated on p-type Si(100).[34] In these experiments, we found that the thickness of the polypyrrole film can be used to control the size and number density of the cubic Cu NPs. Additional advantage in electrodeposition lies in the "fast" synthesis of NPs on the substrate. While all other synthesis techniques take minutes to hours, we show here that the growth of Cu−Cu_2O core−shell NPs can be completed in just a few seconds (<6 s).

For supported NPs, the morphology, number density, and chemical composition all play important roles in their reactivity and selectivity. Depending on the intended application of these NPs, a number of physical and chemical techniques have been developed to control different aspects of their properties.[33,34,36,42,45−47] One particularly important property is the NP shape because the shape of the NP determines how many facets of specific orientation are exposed and therefore available for surface reactions. Given that some planes are more active than the others toward specific chemical reactions,[43] the shape of the NP can have a significant effect on its reactivity and selectivity. Cu and Cu_2O NPs are found to exhibit several different shapes,[48] including asymmetric triangular pyramidal shape with four (111) facets,[36] cubic with six (100) facets,[17,32] cuboctahedral with eight (111) and six (100) facets,[49] and octahedral with eight (111) facets.[35] Since the surface energy of a solid is anisotropic, the shape of a NP is derived by exposing the limiting planes with the lowest free energies at specific concentration and temperature, while the other nonlimiting planes grow faster and are not exposed.[50] Controlling factors that affect the growth kinetics of specific planes will therefore allow us to control the shape of the NP.

In the present work, we investigate fast growth of Cu−Cu_2O core−shell NPs on a H-terminated p-type Si(100) substrate using a one-step, templateless, and capping-agent-free electrodeposition technique. The chemical composition and the crystal structure of these Cu−Cu_2O core−shell NPs have been characterized by depth-profiling X-ray photoelectron spectroscopy (XPS) and glancing-incidence X-ray diffraction (GIXRD). By varying the Cu electrolyte concentration and deposition time, we could control Cu−Cu_2O NPs with three well-defined shapes, an average size range of 5−400 nm, and a range of number densities. The shape evolution as a function of electrolyte concentration can be qualitatively understood in terms of the interplay between the growth kinetics along different facet planes of Cu and the supersaturation factor.[50] The present demonstration work could be extended to the development of better catalysts, selective functionalization on different metal facets, hybrid metallic alloys, and other important application areas discussed above.

RESULTS AND DISCUSSION

Shape Control of Cu−Cu_2O Core−Shell NPs Electrodeposited on H-Si(100). The shape of a Cu−Cu_2O core−shell NP is primarily determined by the initial shape of the Cu core that nucleates on the silicon surface during the deposition process. The deposition of metal NPs onto a support from a solution involves nucleation, followed by diffusion-limited growth, both of which affect the particle size distribution and number density.[45] The nature of both the metal and the support determines not only whether nucleation will be progressive or instantaneous but also whether the growth will follow the Frank−van der Merwe (layer-by-layer) or Volmer−Weber (island) or Stranski−Krastanov (mixed layer and island) growth mode.[40] It is well-known that the nucleation of Cu on Si single crystals (both n-type and p-type) is progressive,[45] which is reflected by the increasing number density with deposition time.[44,45] Cu NPs follow the Volmer−Weber growth mode due to the weak interaction between Cu and Si,[45] which results in in-

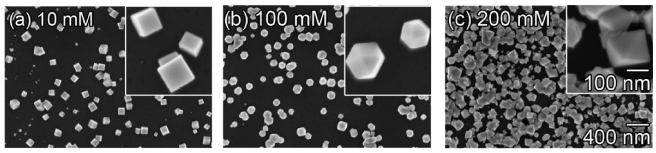

Figure 1. SEM images of Cu−Cu_2O core−shell nanoparticles electrodeposited on H-Si(100) at −1.0 V in an aqueous solution of 10 mM [$NaClO_4$] and [$CuSO_4 \cdot 5H_2O$] of (a) 10 mM for 4 s, (b) 100 mM for 1 s, and (c) 200 mM for 3 s, illustrating their cubic, cuboctahedral, and octahedral shapes.

creasing average particle size with deposition time. During the deposition process, the shape of the NP is known to be determined by the limiting planes with the slower growth rates, which are the (100) and (111) planes for Cu.[50] The difference in the growth rates between the limiting planes causes specific facets to be exposed, producing the shape of the NP.[50] By choosing appropriate kinetic conditions that affect the growth rates of these limiting planes, it is possible to control the shape of the Cu NPs. Subsequently, the outer layers of Cu NPs are converted to Cu_2O in the presence of the aqueous electrolyte used during the electrodeposition, resulting in Cu−Cu_2O core−shell NPs.

Figure 1 shows the scanning electron microscopy (SEM) images of Cu−Cu_2O core−shell NPs of specific shapes, obtained by electrodeposition at three different $CuSO_4 \cdot 5H_2O$ concentrations with appropriately chosen deposition times. At 10 mM [$CuSO_4 \cdot 5H_2O$], well-defined cubic NPs with an average size (edge length) of 90 nm were obtained (Figure 1a), while the shape of the NPs becomes cuboctahedral with an average size [face diagonal of the (100) facet] of 150 nm at 100 mM (Figure 1b) and octahedral with an average size (equatorial edge length) of 200 nm at 200 mM (Figure 1c). It should be noted that the deposition time does not affect the shape of the resulting NPs and is chosen here to provide better illustration of the homogeneous deposition at a selected [$CuSO_4 \cdot 5H_2O$] concentration. Furthermore, a continuous evolution in the shape of the NPs among these three observed shapes occurs among the key [$CuSO_4 \cdot 5H_2O$] concentrations at which the NPs of particular shapes are formed. For example, between 10 and 50 mM [$CuSO_4 \cdot 5H_2O$], NPs of truncated cuboctahedral shapes evolve from a primarily cubic shape at 10 mM to a largely cuboctahedral shape at 50 mM, resulting in a mixture of truncated cubic and cuboctahedral shaped NPs at different stages of growth.

The formation of different shapes of Cu NPs is previously attributed to the role of capping agents. The mechanism proposed by Pileni and co-workers involves initial formation of a decahedral, cuboctahedral, or tetrahedral precursor, followed by preferential adsorption of the capping agents on the nanocrystal facets in order to control the respective growth rates kinetically.[51] Similar growth has recently been observed by Mott *et al.*,[22] supporting the proposed mechanism. However, in their study of cubic NP growth, Gou *et al.* suggested that the capping groups on the Cu_2O surface are not particularly selective to adsorption on different crystal faces.[16] The present result illustrates that, even in the absence of any capping agents, it is possible to grow Cu−Cu_2O core−shell NPs with different shapes. The deposition and growth kinetics during electrodeposition from electrolytes of different concentrations are believed to play an especially important role in forming different shapes of the NPs. In general, particles tend to grow in the directions of planes with a high surface free energy, in order to reduce the surface free energy for the NP by eliminating these planes.[50] The growth rate in the [110] direction of a NP is usually fast because the (110) plane has the highest free energy.[50] The change in shape at different [$CuSO_4 \cdot 5H_2O$] concentrations is the result of changes in the growth rates in the [111] and [100] directions. At a low concentration (5−10 mM [$CuSO_4 \cdot 5H_2O$]), the growth rate of the emerging particle in the [111] direction is faster than that in the [100] direction, resulting in the exposure of the (100) facets. Since a face-centered cubic crystal has six (100) facets, the Cu NPs therefore appear cubic on average in this concentration range. By increasing the concentration to 50 mM, the growth rate in the [100] direction increases and becomes comparable with that in the [111] direction. In this case, the (111) facets start to appear, along with the (100) facets. The cubic shape, with six (100) facets, first changes to truncated octahedron with six octagonal (100) facets and eight triangular (111) facets, and then to cuboctahedron with six square (100) facets and eight triangular (111) facets. At still higher concentrations to 200 mM, the growth rate of the NPs in the [100] direction exceeds that in the [111] direction, and the (111) facets become dominant. The particles become first truncated octahedral with (100) facets at the corners and (111) facets at the edges, then change to octahedral with eight (111) facets. Figure 2 summa-

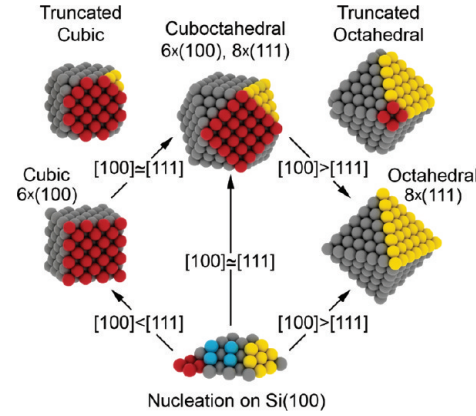

Figure 2. Schematic diagram of the shape evolution of Cu nanoparticles at different relative growth rates along the [100] and [111] directions.

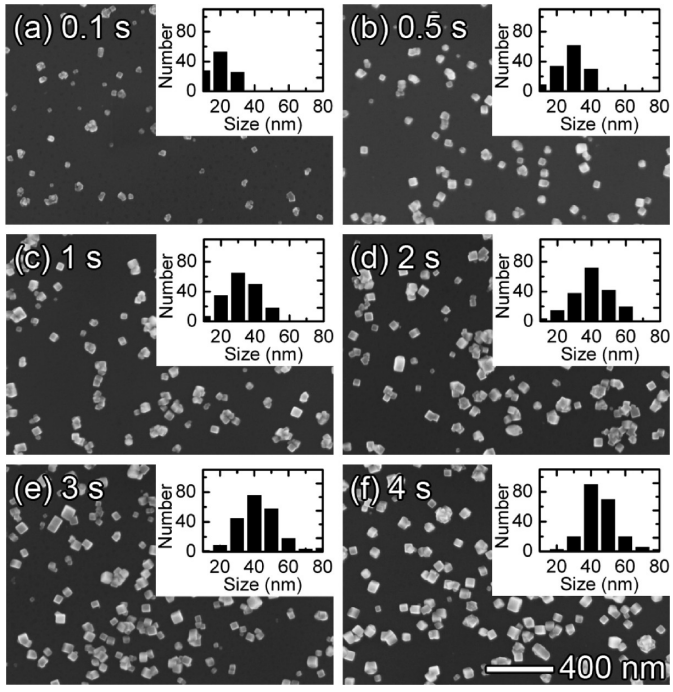

Figure 3. SEM images and size distributions (insets) of Cu−Cu_2O core−shell cubic nanoparticles electrodeposited on H-Si(100) at −1.0 V in an aqueous solution of 5 mM [$CuSO_4 \cdot 5H_2O$] (and 10 mM [$NaClO_4$]) for deposition times of (a) 0.1 s, (b) 0.5 s, (c) 1 s, (d) 2 s, (e) 3 s, and (f) 4 s.

rizes the growth evolution of different shapes of NPs depending on the relative growth rates along the [100] and [111] directions.

Size and Number Density of Cu−Cu_2O Core−Shell Nanoparticles of Specific Shapes. For NPs of a particular shape obtained in a specific [$CuSO_4 \cdot 5H_2O$] range, it is possible to control the size distribution and number density by varying the deposition time. Figure 3 shows that both the average size (edge length) and the number density of the cubic NPs obtained at 5 mM [$CuSO_4 \cdot 5H_2O$] increase with increasing deposition time. From 0.1 to 0.5 s deposition time, the NPs increase in average size from 20 nm with a size range of 0−40 nm (Figure 3a) to 30 nm with a range of 10−50 nm (Figure 3b). Increasing the deposition time to 1.0 and 2.0 s causes the average size to increase to 30 and 40 nm, respectively, with respective size ranges of 5−60 and 10−70 nm (Figure 3c,d). Above 2.0 s deposition time (Figure 3e,f), the average size remains effectively unchanged as the particle approaches the optimum average size of 40−45 nm. The corresponding size distribution evidently becomes narrower; that is, the particles become more uniform in size (from 15−65 nm for 3.0 s to 25−65 nm for 4.0 s). Further increase in the deposition time causes the particles to cluster and coalesce, producing a thin film (not shown). As shown in Figure 4, similar dependence of the particle size on the deposition time can also be observed for NPs with different shapes obtained at different [$CuSO_4 \cdot 5H_2O$] concentrations, that is, among NPs of cubic (10 mM), cuboctahedral (50 mM), and octahedral shapes (200 mM). In addition, the number density of NPs is also found to increase with increasing deposition time, as shown for cubic NPs in Figure 3. For a longer deposition time, the number density increases until the NPs start to coalesce to bigger NPs, as found in Ostwald ripening (and eventually forming a film). These changes are illustrated for cuboctahedral NPs in Figure 5, and they are consistent with progressive nucleation of the Cu NP growth on H-Si(100).

The dependence of the NP size can be understood in terms of the supersaturation factor, which is defined as the ratio of the actual pressure experienced by the growing particle at a particular size to that at the optimum size at specific concentration and temperature.[50] If the supersaturation factor is greater than 1, the NP will continue to grow until it reaches the optimum size with a unity factor, at which point the particle growth stops. By increasing the deposition time, the amount of charge transfer increases, increasing the particle size, which in turn causes the surface area to increase and the pressure to decrease. As a result, the supersaturation factor decreases and becomes closer to 1, with the particle size approaching the optimum size at that concentration. Because the nucleation process of Cu NPs on the Si surface is progressive, new nucleation sites are created continuously (as long as there is open space on the substrate), increasing the number density, during the electrodeposition process. The NPs that nucleate first will therefore have the largest size, and they will reach the optimum size first and stop growing. As the

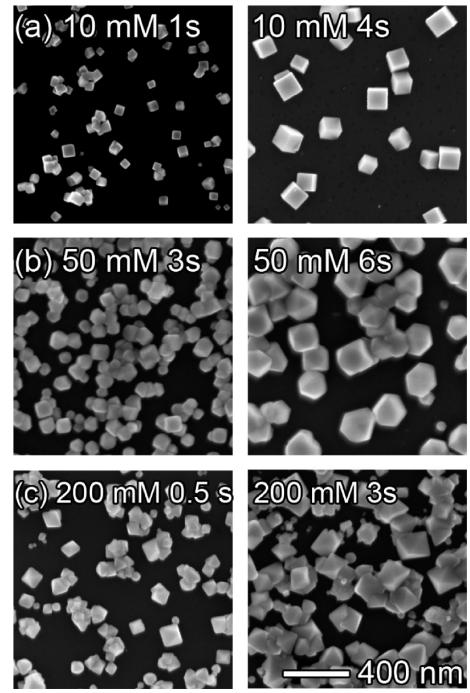

Figure 4. SEM images of cubic, cuboctahedral, and octahedral Cu−Cu_2O core−shell nanoparticles electrodeposited on H-Si(100) at −1.0 V in respective aqueous solutions of (a) 10 mM, (b) 50 mM, and (c) 200 mM [$CuSO_4 \cdot 5H_2O$] (and 10 mM [$NaClO_4$]), each for two different deposition times.

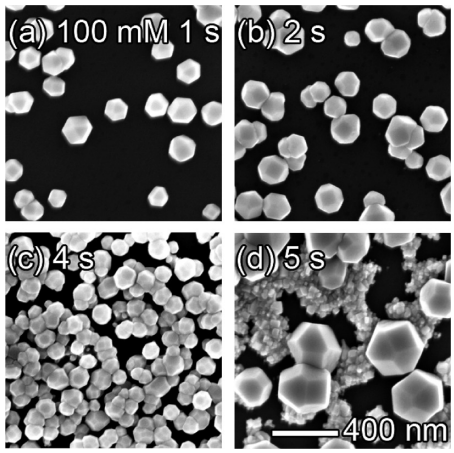

Figure 5. SEM images of Cu−Cu_2O core−shell cuboctahedral nanoparticles electrodeposited on H-Si(100) at −1.0 V in an aqueous solution of 100 mM [$CuSO_4 \cdot 5H_2O$] (and 10 mM [$NaClO_4$]) for deposition times of (a) 1 s, (b) 2 s, (c) 4 s, and (d) 5 s.

deposition continues, nucleation of the NPs will eventually cover the entire surface, saturating the number density and further limiting creation of new particles. The size distribution will become narrower if a sufficient amount of deposition time is provided for all the nucleated particles to grow bigger and reach the optimum size, as illustrated in Figure 3. When most of the particles reach the optimum size at a specific concentration, further deposition will cause the particles to coalesce, producing Oswald ripening and/or film formation, as shown in Figure 5.

Crystal Structure and Chemical Composition. Figure 6 shows the GIXRD spectra for cubic, cuboctahedral, and octahedral Cu−Cu_2O core−shell NPs electrodeposited on H-Si(100) at −1.0 V. The prominent peaks at 43.30, 50.43, and 74.24° correspond, respectively, to the (111), (200), and (220) of face-centered cubic Cu (with space group *Fm*3$\bar{m}$, JCPDS 01-070-3039), and the weaker features at 36.42, 42.30, 61.35, and 73.53° can be assigned to the (111), (200), (220), and (311) of simple cubic Cu_2O (with space group *Pn*3$\bar{m}$, JCPDS 00-077-0199).[52] The overall diffraction intensity from the Cu phase is found to be higher than that from the Cu_2O phase for octahedral and cuboctahedral NPs, indicating a higher quantity of Cu in these individual NPs. For cubic NPs, the Cu_2O intensity is higher than that of Cu, consistent with the larger Cu_2O (shell) relative composition in this smallest NP. The similar GIXRD patterns observed for NPs of different shapes suggest the same crystal structure with major crystal planes diffracting at essentially the same 2θ angles. Moreover, there is a marked difference in the relative intensities of the (111) features for both the Cu_2O and Cu phases. As discussed in the mechanism of NP shape evolution, increasing the $CuSO_4 \cdot 5H_2O$ concentration (from 10 to 100 to 200 mM) would decrease the growth rate of the (111) plane of the Cu core, thereby reducing the amount of (111) facets. This is clearly reflected by the observed decrease in the Cu(111) diffraction intensity from octahedral to cuboctahedral to cubic NPs.

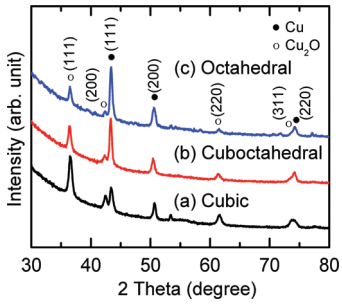

Figure 6. Glancing-incidence XRD pattern of Cu−Cu_2O core−shell (a) cubic, (b) cuboctahedral, and (c) octahedral nanoparticles electrodeposited on H-Si(100) at −1.0 V in an aqueous solution of 10, 100, and 200 mM [$CuSO_4 \cdot 5H_2O$] (and 10 mM [$NaClO_4$]) for 30, 30, and 15 s deposition time, respectively.

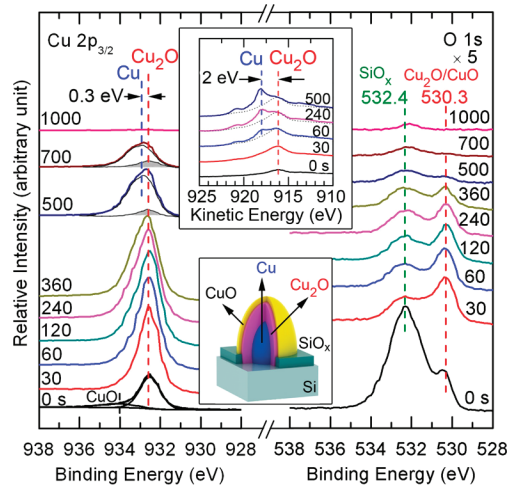

Figure 7. XPS spectra of Cu $2p_{3/2}$ and O 1s regions of Cu−Cu_2O core−shell cubic nanoparticles electrodeposited on H-Si(100) at −1.0 V in an aqueous solution of 10 mM [$CuSO_4 \cdot 5H_2O$] (and 10 mM [$NaClO_4$]) for 4 s deposition time and upon sputtering for selected times. The insets show the corresponding Cu LMM Auger features and a schematic model of the core−shell nanoparticle.

Figure 7 shows typical XPS spectra for the Cu $2p_{3/2}$ and O 1s regions at different sputtering times for cubic Cu−Cu_2O core−shell NPs obtained at 10 mM [$CuSO_4 \cdot 5H_2O$] for 4 s (Figure 4a). For the as-deposited sample, the peak at 932.6 eV can be attributed to Cu_2O, in accord with the literature data.[53,54] The presence of a very weak but discernible Cu $2p_{3/2}$ peak at 934.0 eV (Figure 7) and its satellite peak at 942.0 eV (not shown) can be assigned to CuO.[55] This overlayer is evidently removed after a short sputtering of 30−60 s, which indicates that the CuO overlayer is quite thin (<2 nm). The marked increase in the intensity of the Cu_2O feature at 932.6 eV after 30 s of sputtering could be due to the removal of a carbonaceous layer often found in sample handling under ambient conditions. The Cu $2p_{3/2}$ spectrum appears essentially unchanged after further sputtering for 240 s, above which peak broadening and intensity reduction are observed. After 500 s of

sputtering, we observe the emergence of additional intensity at 932.9 eV (*i.e.*, 0.3 eV higher in binding energy than the Cu_2O feature) by peak deconvolution, corresponding to metallic Cu.[53,54] The presence of the metallic Cu feature is better illustrated in the corresponding Cu LMM Auger spectra (Figure 7, inset). In particular, the metallic Cu Auger feature at 918.0 eV kinetic energy[53,54] is clearly evident after sputtering for just 60 s, and this metallic feature becomes more intense with further sputtering while the corresponding Cu_2O Auger feature at 916.0 eV kinetic energy[53,54] weakens. The Cu Auger spectra therefore confirm that the Cu NP consists of a metallic Cu core and a Cu_2O shell with a thin outer-layer of CuO as indicated in the XPS spectra.

The corresponding O 1s spectrum for the as-deposited sample shows two peaks at 532.4 and 530.3 eV, attributed to amorphous silicon oxide (SiO_x) and Cu oxides (Cu_2O/CuO), respectively.[56−58] The presence of the strong SiO_x O 1s feature is due to in-solution oxidation of the Si surface not covered by the Cu NPs during the electrodeposition process. After 30 s of sputtering, the SiO_x feature is significantly reduced, making the Cu oxide feature at 530.3 eV more evident. Further sputtering reduces the intensities of both features, with complete removal of the Cu oxide features after 500 s. The remaining intensity at 532.4 eV corresponds to oxygen inside the bulk Si. It should be noted that, after the complete removal of the Cu oxide O 1s feature at 530.3 eV, considerable intensity for the Cu $2p_{3/2}$ feature at 932.9 eV is clearly observed. This marks the complete removal of the Cu_2O shell and the presence of Cu NPs with just the metallic Cu core. It should also be noted that the small shift in Cu $2p_{3/2}$ binding energy found for the metallic Cu core could also indicate a quantum size effect. In particular, the depth-profiling XPS measurement for a Cu film on Si(100) by Paszti *et al.*[37] showed that the Cu $2p_{3/2}$ peak broadens and shifts by 0.4 eV, which they attributed to a quantum size effect. Finally, we also find similar depth profiles for cuboctahedral and octahedral Cu NPs obtained with different deposition conditions, which confirms the "universal" core−shell nature of these electrochemically deposited Cu NPs.

On the basis of the GIXRD and depth-profiling XPS data, we propose a general core−shell model, shown in Figure 8, for the Cu NPs of different shapes and crystal structures electrodeposited on H-Si(100). The formation of Cu_2O shell on the Cu core is attributed to the use of aqueous electrolyte solution, while a thin CuO outerlayer could also be formed when samples were taken to ambient conditions.

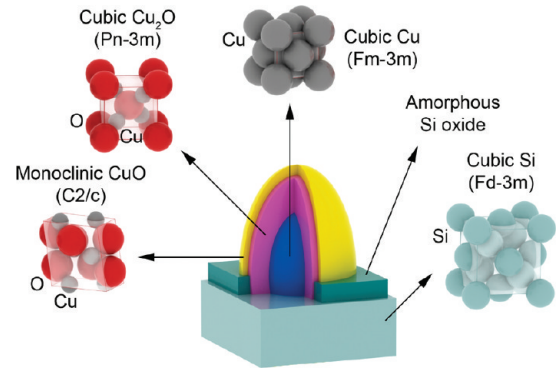

Figure 8. Schematic model for Cu nanoparticles electrodeposited on Si(100), depicting the metallic Cu core and Cu_2O shell with a CuO outerlayer. This model is based on the crystallographic data of refs 59−62.

CONCLUSIONS

The present work shows that Cu−Cu_2O core−shell NPs of cubic, cuboctahedral, octahedral shapes can be obtained by a fast, one-step, templateless, capping-agent-free electrochemical method using the [$CuSO_4 \cdot 5H_2O$] concentration as the control parameter. In particular, cubic NPs with six (100) facets, cuboctahedral NPs with six (100) facets and eight (111) facets, and octahedral NPs with eight (111) facets can be produced with 5−10, 50−100, and 200 mM [$CuSO_4 \cdot 5H_2O$], respectively, in just a few seconds (0.1 to 6 s). A continuous evolution in the shape with truncated crystal structures among these three primary shapes can also be observed at intermediate [$CuSO_4 \cdot 5H_2O$] concentrations. Furthermore, the size and number density of these NPs with specific shapes can also be easily controlled by the deposition time at selected [$CuSO_4 \cdot 5H_2O$] concentrations. Evolution of the average size and distribution, up to a critical dimension, can be understood in terms of the supersaturation factor in the diffusion-limited progressive growth model. Using GIXRD and depth-profiling XPS, we also determine that these NPs, regardless of shapes, consist of a crystalline metallic Cu core and a Cu_2O shell with a thin CuO outerlayer. The ability to control the relative amounts of different (100) and (111) facets over a full range of Cu NPs of different shapes supported on Si(100) provides new opportunity to develop site-specific surface chemistry in emerging applications. Our future work will focus on selective functionalization by organic molecules and hybrid metallic alloy deposition using these NPs as a template substrate.

EXPERIMENTAL DETAILS

Single-side polished B-doped Si(100) wafers (0.40 mm thick) with a resistivity of 1.0−1.5 mΩ · cm were cut into 15 × 2.5 mm^2 rectangular chips. The Si chips were cleaned and H-terminated by using a standard RCA method.[63] A potentio/galvanostat electrochemical workstation (CHI Instrument 660A) with a three-electrode cell (with a Ag/AgCl reference electrode, a platinum wire counter electrode, and the Si chip as the working electrode) was used for the electrodeposition experiments. Cu−Cu_2O core−shell nanocrystals were deposited on the H-terminated

Si(100) chips at room temperature in an aqueous Cu electrolyte solution (without stirring) for a preselected deposition time by amperometry potentiostatically at a constant potential of −1.0 V (with respect to the Ag/AgCl reference electrode). The Cu electrolyte solution consisted of a preselected concentration of $CuSO_4 \cdot 5H_2O$ and a fixed concentration [10 mM] of $NaClO_4$ used as a supporting electrolyte. The electrolyte solution was appropriately deoxygenated by nitrogen bubbling for at least 20 min prior to use.[47] Two deposition parameters were used to produce NPs with different shapes, sizes, and number density. In particular, Cu electrolyte concentrations [$CuSO_4 \cdot 5H_2O$] of 5, 10, 50, 100, 200, and 500 mM and deposition times of 0.1, 0.5, 1, 2, 3, 4, 5, 10, and 20 s were varied in a systematic fashion. The resulting NP-deposited Si substrates were thoroughly rinsed with Millipore water (with a resistively of 18.2 MΩ · cm) and dried for at least 24 h in a nitrogen-purged drying box prior to characterization.

SEM with a LEO FESEM 1530 microscope was used to determine the shape, size, and number density of the Cu−Cu_2O core−shell NPs electrodeposited on the Si(100) chip. The crystal structure of the Cu−Cu_2O core−shell NPs was further characterized with GIXRD using a PANalytical X'Pert Pro MRD diffractometer with Cu Kα radiation (1.54 Å) at an incidence angle of 0.3°. The chemical composition of the Cu−Cu_2O core−shell NPs was analyzed by XPS as a function of sputtering depth (depth profiling) using a Thermo-VG Scientific ESCALab 250 Microprobe with a monochromatic Al Kα source (1486.6 eV), capable of an overall energy resolution of 0.4−0.5 eV full width at half-maximum. Sputtering was performed by rasterring a 3.0 keV Ar^+ ion beam over a 3 × 3 mm^2 area of the sample at a typical sample current density of 102 nA/mm^2.

Acknowledgment. This work was supported by the Natural Sciences and Engineering Research Council of Canada.

REFERENCES AND NOTES

1. Nakatsuji, H.; Hu, Z.-M. Mechanism of Methanol Synthesis on Cu(100) and Zn/Cu(100) Surfaces: Comparative Dipped Adcluster Model Study. *Int. J. Quantum Chem.* **2000**, *77*, 341–349.
2. Ikari, S.; Kashiwade, H.; Matsuoka, T.; Hirayama, T.; Ishida, S.; Kato, K. Improvement of Copper Plating Adhesion of PPE Printed Wiring Board by Plasma Treatment. *Surf. Coat. Technol.* **2008**, *202*, 5583–5585.
3. de Jongh, P. E.; Vanmaekelbergh, D.; Kelly, J. J. Cu_2O: A Catalyst for the Photochemical Decomposition of Water. *Chem. Commun.* **1999**, 1069–1070.
4. Lee, J. K.; Choi, J.; Kang, S. J.; Lee, J. M.; Tak, Y.; Lee, J. Influence of Copper Oxide Modification of a Platinum Cathode on the Activity of Direct Methanol Fuel Cell. *Electrochim. Acta* **2007**, *52*, 2272–2276.
5. Akimoto, K.; Ishizuka, S.; Yanagita, M.; Nawa, Y.; Paul, G. K.; Sakurai, T. Thin Film Deposition of Cu_2O and Application for Solar Cells. *Sol. Energy* **2006**, *80*, 715–722.
6. Tamaki, J.; Shimanoe, K.; Yamada, Y.; Yamamoto, Y.; Miura, N.; Yamazoe, N. Dilute Hydrogen Sulfide Sensing Properties of CuO−SnO_2 Thin Film Prepared by Low-Pressure Evaporation Method. *Sens. Actuators, B* **1998**, *49*, 121–125.
7. Zhang, H.; Zhu, Q.; Zhang, Y.; Wang, Y.; Zhao, L.; Yu, B. One-Pot Synthesis and Hierarchical Assembly of Hollow Cu_2O Microspheres with Nanocrystals-Composed Porous Multishell and Their Gas-Sensing Properties. *Adv. Funct. Mater.* **2007**, *17*, 2766–2771.
8. Ishihara, T.; Higuchi, M.; Takagi, T.; Ito, M.; Nishiguchi, H.; Takita, Y. Preparation of CuO Thin Films on Porous $BaTiO_3$ by Self-Assembled Multibilayer Film Formation and Application as a CO_2 Sensor. *J. Mater. Chem.* **1998**, *8*, 2037–2042.
9. Borkow, G.; Sidwell, R. W.; Smee, D. F.; Barnard, D. L.; Morrey, J. D.; Lara-Villegas, H. H.; Shemer-Avni, Y.; Gabbay, J. Neutralizing Viruses in Suspensions by Copper Oxide-Based Filters. *Antimicrob. Agents Chemother.* **2007**, *51*, 2605–2607.
10. Borkow, G.; Lara, H. H.; Covington, C. Y.; Nyamathi, A.; Gabbay, J. Deactivation of Human Immunodeficiency Virus Type 1 in Medium by Copper Oxide-Containing Filters. *Antimicrob. Agents Chemother.* **2008**, *52*, 518–525.
11. Barreca, D.; Gasparotto, A.; Maccato, C.; Tondello, E.; Lebedev, O. I.; Van Tendeloo, G. CVD of Copper Oxides from a β-Diketonate Diamine Precursor: Tailoring the Nano-Organization. *Cryst. Growth Des.* **2009**, *9*, 2470–2480.
12. Pászti, Z.; Petö, G.; Horváth, Z. E.; Karacs, A. Laser Ablation Induced Formation of Nanoparticles and Nanocrystal Networks. *Appl. Surf. Sci.* **2000**, *168*, 114–117.
13. van der Grift, C. J. G.; Mulder, A.; Geus, J. W. The Sol−Gel Preparation of Porous Catalyst Spheres. *Colloids Surf. B* **1991**, *53*, 223–240.
14. Radwan, N. R. E.; El-Shall, M. S.; Hassan, H. M. A. Synthesis and Characterization of Nanoparticle Co_3O_4, CuO and NiO Catalysts Prepared by Physical and Chemical Methods to Minimize Air Pollution. *Appl. Catal., A* **2007**, *331*, 8–18.
15. Zhao, H. Y.; Wang, Y. F.; Zeng, J. H. Hydrothermal Synthesis of Uniform Cuprous Oxide Microcrystals with Controlled Morphology. *Cryst. Growth Des.* **2008**, *8*, 3731–3734.
16. Gou, L.; Murphy, C. J. Controlling the Size of Cu_2O Nanocubes from 200 to 25 nm. *J. Mater. Chem.* **2004**, *14*, 735–738.
17. Gou, L.; Murphy, C. J. Solution-Phase Synthesis of Cu_2O Nanocubes. *Nano Lett.* **2003**, *3*, 231–234.
18. Brege, J. J.; Hamilton, C. E.; Crouse, C. A.; Barron, A. R. Ultrasmall Copper Nanoparticles from a Hydrophobically Immobilized Surfactant Template. *Nano Lett.* **2009**, *9*, 2239–2242.
19. Yen, M.-Y.; Chiu, C.-W.; Chen, F.-R.; Kai, J.-J.; Lee, C.-Y.; Chiu, H.-T. Convergent Electron Beam Induced Growth of Copper Nanostructures: Evidence of the Importance of a Soft Template. *Langmuir* **2004**, *20*, 279–281.
20. Tanori, J.; Pileni, M. P. Control of the Shape of Copper Metallic Particles by Using a Colloidal System as Template. *Langmuir* **1997**, *13*, 639–646.
21. Zhang, H.; Cui, Z. Solution-Phase Synthesis of Smaller Cuprous Oxide Nanocubes. *Mater. Res. Bull.* **2008**, *43*, 1583–1589.
22. Mott, D.; Galkowski, J.; Wang, L.; Luo, J.; Zhong, C.-J. Synthesis of Size-Controlled and Shaped Copper Nanoparticles. *Langmuir* **2007**, *23*, 5740–5745.
23. Long, J.; Dong, J.; Wang, X.; Ding, Z.; Zhang, Z.; Wu, L.; Li, Z.; Fu, X. Photochemical Synthesis of Submicron- and Nano-scale Cu_2O Particles. *J. Colloid Interface Sci.* **2009**, *333*, 791–799.
24. Lee, Y.; Choi, J.; Lee, K. J.; Stott, N. E.; Kim, D. Large-Scale Synthesis of Copper Nanoparticles by Chemically Controlled Reduction for Applications of Inkjet-Printed Electronics. *Nanotechnology* **2008**, *19*, 415604/1–415604/7.
25. Dhas, N. A.; Raj, C. P.; Gedanken, A. Synthesis, Characterization, and Properties of Metallic Copper Nanoparticles. *Chem. Mater.* **1998**, *10*, 1446–1452.
26. Liu, Y.-C.; Yang, K.-H.; Ger, M.-D. Mechanism of Underpotential Deposition of Metal on Conducting Polymers. *Synth. Met.* **2002**, *126*, 337–345.
27. Guascito, M. R.; Boffi, P.; Malitesta, C.; Sabbatini, L.; Zambonin, P. G. Conducting Polymer Electrodes Modified by Metallic Species for Electrocatalytic Purposes—Spectroscopic and Microscopic Characterization. *Mater. Chem. Phys.* **1996**, *44*, 17–24.
28. Cioffi, N.; Torsi, L.; Losito, I.; Di Franco, C.; Di Bari, I.; Chiavarone, L.; Scamarcio, G.; Tsakova, V.; Sabbatini, L.; Zambonin, P. G. Electrosynthesis and Analytical Characterisation of Polypyrrole Thin Films Modified with Copper Nanoparticles. *J. Mater. Chem.* **2001**, *11*, 1434–1440.
29. Makhloufi, L.; Hammache, H.; Saidani, B.; Akilal, N.; Maloum, Y. Preparation on Iron of a Polypyrrole (PPy) Electrode Modified with Copper by the Electrochemical Cementation Process. *J. Appl. Electrochem.* **2000**, *30*, 1143–1150.
30. Tsakova, V.; Borissov, D.; Ranguelov, B.; Stromberg, Ch.;

Schultze, J. W. Electrochemical Incorporation of Copper in Polyaniline Layers. *Electrochim. Acta* **2001**, *46*, 4213–4222.
31. Tsakova, V.; Borissov, D. Electrochemical Deposition of Copper in Polyaniline Films—Number Density and Spatial Distribution of Deposited Metal Clusters. *Electrochem. Commun.* **2000**, *2*, 511–515.
32. Sarkar, D. K.; Zhou, X. J.; Tannous, A.; Louie, M.; Leung, K. T. Growth of Self-Assembled Copper Nanostructure on Conducting Polymer by Electrodeposition. *Solid State Commun.* **2003**, *125*, 365–368.
33. Sarkar, D. K.; Zhou, X. J.; Tannous, A.; Leung, K. T. Growth Mechanisms of Copper Nanocrystals on Thin Polypyrrole Films by Electrochemistry. *J. Phys. Chem. B* **2003**, *107*, 2879–2881.
34. Zhou, X. J.; Harmer, A.; Heinig, N.; Leung, K. T. Parametric Study on Electrochemical Deposition of Copper Nanoparticles on an Ultrathin Polypyrrole Film Deposited on a Gold Film Electrode. *Langmuir* **2004**, *20*, 5109–5113.
35. Tang, S. C.; Meng, X. K.; Vongehr, S. An Additive-Free Electrochemical Route to Rapid Synthesis of Large-Area Copper Nano-octahedra on Gold Film Substrates. *Electrochem. Commun.* **2009**, *11*, 867–870.
36. Ko, W.-Y.; Chen, W.-H.; Tzeng, S.-D.; Gwo, S.; Lin, K.-J. Synthesis of Pyramidal Copper Nanoparticles on Gold Substrate. *Chem. Mater.* **2006**, *18*, 6097–6099.
37. Pászti, Z.; Petöe, G.; Horváth, Z. E.; Karacs, A.; Guczi, L. Formation and Valence Band Density of States of Nonspherical Cu Nanoparticles Deposited on Si(100) Substrate. *J. Phys. Chem. B* **1997**, *101*, 2109–2115.
38. Khelladi, M. R.; Mentar, L.; Azizi, A.; Sahari, A.; Kahoul, A. Electrochemical Nucleation and Growth of Copper Deposition onto FTO and n-Si(100) Electrodes. *Mater. Chem. Phys.* **2009**, *115*, 385–390.
39. Shao, W.; Pattanaik, G.; Zangari, G. Electrochemical Nucleation and Growth of Copper from Acidic Sulfate Electrolytes on n-Si(001): Effect of Chloride Ions. *J. Electrochem. Soc.* **2007**, *154*, D339–D345.
40. Ji, C.; Oskam, G.; Searson, P. C. Electrochemical Nucleation and Growth of Copper on Si(111). *Surf. Sci.* **2001**, *492*, 115–124.
41. Radisic, A.; West, A. C.; Searson, P. C. Influence of Additives on Nucleation and Growth of Copper on n-Si(111) from Acidic Sulfate Solutions. *J. Electrochem. Soc.* **2002**, *149*, C94–C99.
42. Ji, C.; Oskam, G.; Searson, P. C. Electrodeposition of Copper on Silicon from Sulfate Solution. *J. Electrochem. Soc.* **2001**, *148*, C746–C752.
43. Xu, H.; Wang, W.; Zhu, W. Shape Evolution and Size-Controllable Synthesis of Cu_2O Octahedra and Their Morphology-Dependent Photocatalytic Properties. *J. Phys. Chem. B* **2006**, *110*, 13829–13834.
44. Feldheim, D.; Foss, C. *Metal Nanoparticles, Synthesis, Characteristics and Applications*; Marcel Dekker: New York, 2002.
45. Oskam, G.; Long, J. G.; Natarajan, A.; Searson, P. C. Electrochemical Deposition of Metals onto Silicon. *J. Phys. D* **1998**, *31*, 1927–1949.
46. Grujicic, D.; Pesic, B. Electrodeposition of Copper: The Nucleation Mechanisms. *Electrochim. Acta* **2002**, *47*, 2901–2912.
47. Singh, A.; Luening, K.; Brennan, S.; Homma, T.; Kubo, N.; Pianetta, P. Nucleation and Growth of Copper Nanoparticles on Silicon Surfaces. *Phys. Scr.* **2005**, *T115*, 714–716.
48. Zheng, Z.; Huang, B.; Wang, Z.; Guo, M.; Qin, X.; Zhang, X.; Wang, P.; Dai, Y. Crystal Faces of Cu_2O and Their Stabilities in Photocatalytic Reactions. *J. Phys. Chem. C* **2009**, *113*, 14448–14453.
49. Lisiecki, I. Size, Shape, and Structural Control of Metallic Nanocrystals. *J. Phys. Chem. B* **2005**, *109*, 12231–12244.
50. Henry, C. R. Morphology of Supported Nanoparticles. *Prog. Surf. Sci.* **2005**, *80*, 92–116.
51. Salzemann, C.; Lisiecki, I.; Urban, J.; Pileni, M.-P. Anisotropic Copper Nanocrystals Synthesized in a Supersaturated Medium: Nanocrystal Growth. *Langmuir* **2004**, *20*, 11772–11777.
52. PDF-2 Database, *International Center for Diffraction Data*, **2004**.
53. Stefanov, P.; Marinova, Ts. Adsorption of Oxygen and Formation of an Oxide Phase on a Cu(100) Surface. *Appl. Surf. Sci.* **1988**, *31*, 445–450.
54. Panzner, G.; Egert, B.; Schmidt, H. P. The Stability of Cupric Oxide and Cuprous Oxide Surfaces during Argon Sputtering Studied by XPS and AES. *Surf. Sci.* **1985**, *151*, 400–408.
55. Balamurugan, B.; Mehta, B. R.; Shivaprasad, S. M. Surface-Modified CuO Layer in Size-Stabilized Single-Phase Cu_2O Nanoparticles. *Appl. Phys. Lett.* **2001**, *79*, 3176–3178.
56. Sung, M. M.; Sung, K.; Kim, C. G.; Lee, S. S.; Kim, Y. Self-Assembled Monolayers of Alkanethiols on Oxidized Copper Surfaces. *J. Phys. Chem. B* **2000**, *104*, 2273–2277.
57. Fleisch, T. H.; Mains, G. J. Reduction of Copper Oxides by UV Radiation and Atomic Hydrogen Studied by XPS. *Appl. Surf. Sci.* **1982**, *10*, 51–62.
58. Ghijsen, J.; Tjeng, L. H.; van Elp, J.; Eskes, H.; Westerink, J.; Sawatzky, G. A.; Czyzyk, M. T. Electronic Structure of Cuprous and Cupric Oxides. *Phys. Rev. B* **1988**, *38*, 11322–11330.
59. Suh, I. K.; Ohta, H.; Waseda, Y. High-Temperature Thermal Expansion of Six Metallic Elements Measured by Dilatation Method and X-ray Diffraction. *J. Mater. Sci.* **1988**, *23*, 757–760.
60. Kirfel, A.; Eichhorn, K. Accurate Structure Analysis with Synchrotron Radiation. The Electron Density in Al_2O_3 and Cu_2O. *Acta Crystallogr.* **1990**, *A46*, 271–284.
61. Celotti, G.; Nobili, D.; Ostoja, P. Lattice Parameter Study of Silicon Uniformly Doped with Boron and Phosphorus. *J. Mater. Sci.* **1974**, *9*, 821–828.
62. Calos, N. J.; Forrester, J. S.; Schaffer, G. B. A Crystallographic Contribution to the Mechanism of a Mechanically Induced Solid State Reaction. *J. Solid State Chem.* **1996**, *122*, 273–280.
63. Kern, W.; Puotinen, D. A. Cleaning Solution Based on Hydrogen Peroxide for Use in Silicon Semiconductor Technology. *RCA Rev.* **1970**, *31*, 187–206.